Density functional theory calculations of mechanical and electronic properties of $W_{1-x}Ta_xN_6$, $W_{1-x}Mo_xN_6$, and $Mo_{1-x}Ta_xN_6$ ($0 \leq x \leq 1$) alloys in hexagonal structure

S. R. Kandel[a,*], D. Gall[b], S. V. Khare[a]

[a]Department of Physics and Astronomy, University of Toledo, Toledo, OH 43606, USA

[b]Department of Materials Science and Engineering, Rensselaer Polytechnic Institute, Troy, NY 12180, USA

*Corresponding Author: shreedhar.kandel@rockets.utoledo.edu

Abstract

We report structural, energetic, mechanical, electronic, thermal, and magnetic properties of $W_{1-x}Ta_xN_6$, $W_{1-x}Mo_xN_6$, and $Mo_{1-x}Ta_xN_6$ ($0 \leq x \leq 1$) alloys in the hexagonal structure (space group: $R\bar{3}m$) determined using density functional theory based first principles calculations. These compounds are mechanically stable whereas $W_{0.33}Ta_{0.66}N_6$ is vibrationally unstable. Among both mechanically and vibrationally stable compounds, $W_{0.66}Ta_{0.33}N_6$ and $W_{0.66}Mo_{0.33}N_6$ have the highest hardness of 55 GPa while the softest alloy ($Mo_{0.33}Ta_{0.66}N_6$) exhibits 46 GPa, indicating new potential super hard materials. The high hardness in these materials is attributed to the combined effect of covalent N-N bonding of hexagonal rings and a metal to nitrogen charge transfer. Only two alloys $W_{0.33}Mo_{0.66}N_6$ and $W_{0.66}Mo_{0.33}N_6$ are semiconducting with electronic band gaps of 1.82 and 1.92 eV, respectively. A significant magnetic moment of 0.82 μ_B per unit metal was calculated for $W_{0.66}Mo_{0.33}N_6$.

Keywords: Transition metal nitrides, Density functional theory, Super hard alloys, Electronic properties, Vibrational properties.

I. INTRODUCTION

Transition metal nitrides (TMNs) are known to have excellent mechanical properties (high hardness) as well as chemical and thermal properties making them suitable candidates for hard coating materials[1-9]. Results from the experimentally synthesized TMNs have also verified the theoretically predicted values of hardness for these materials[10-15]. Recently, binary super hard TMNs in hexagonal phase of WN_6, MoN_6, and TaN_6 (space group: $R\bar{3}m$) have also been predicted by employing the first principles-based calculations and machine learning approaches[16-18]. The predicted Vickers hardness (H_V) of these nitrides are reported to be 59 GPa (WN_6), 52 GPa (MoN_6), and 43 GPa (TaN_6)[16]. Such outstanding hardnesses of these nitrides make them suitable for hard coatings, a further study of their alloys in the same crystal structure (space group: $R\bar{3}m$) cannot be overlooked[19, 20].

In this study, density functional theory (DFT) is employed to investigate the mechanical and electronic properties of $W_{1-x}Ta_xN_6$, $W_{1-x}Mo_xN_6$, and $Mo_{1-x}Ta_xN_6$ ($0 \leq x \leq 1$) alloys. We found the compounds are mechanically stable, however, $W_{0.33}Ta_{0.66}N_6$ has unstable phonon frequencies. In addition, energetic, structural, magnetic, and thermal properties are also investigated. $W_{0.66}Ta_{0.33}N_6$ and $W_{0.66}Mo_{0.33}N_6$ are predicted to be the hardest compounds with calculated $H_V = 55$ GPa for each while $Mo_{0.33}Ta_{0.66}N_6$ is the softest material with $H_V = 46$ GPa among alloys. Thus, with the observed high hardness values, these alloys may be labelled as potential new super hard materials. The study of local density of states (LDOS) reveals that most of the alloy are metallic. The metallic nature can also be verified from the band structure analysis where only two compounds are showing a band gap. The calculated band gaps are 1.36 eV ($W_{0.33}Mo_{0.66}N_6$) and 1.40 eV ($W_{0.66}Mo_{0.33}N_6$) respectively. Since band gap calculation using generalized gradient approximation functionals tends to underestimate it[21], the corrected band gaps using hybrid

functional calculations for the same materials are calculated to be 1.82 eV ($W_{0.33}Mo_{0.66}N_6$) and 1.92 eV ($W_{0.66}Mo_{0.33}N_6$). The charge transfer from metal to nitrogen indicates an existence of ionic bonding. This result is supported by the crystal orbital Hamilton population (COHP) analyses showing the bonding states of metal and nitrogen interaction. We found only one compound ($W_{0.66}Mo_{0.33}N_6$) that is magnetic with magnetic moment per unit metal calculated to be 0.82 μ_B, where μ_B is Bohr magneton.

II. COMPUTATIONAL METHODS

The density functional theory (DFT) based calculations are performed by using Vienna Ab initio Simulation Package (VASP)[4-6, 16, 20, 22-32]. The electron density is approximated by utilizing Projector Augmented Wave (PAW) method within the Generalized Gradient Approximation (GGA) with Perdew-Burke-Ernzerhof (PBE) functional[4, 16, 22, 23, 26, 30, 33-35]. For inner core electrons, VASP pseudopotentials W, Mo, Ta with the inner electrons and N are considered[4, 16, 23, 36, 37]. For relaxation of structure, the plane wave cut-off energy of 600 eV in Γ-centered k-mesh of grid density $6 \times 6 \times 7$ are used. The ionic and electronic convergence criteria of forces and energy are set at 0.01 eV/Å and 10^{-6} eV/atom respectively. The Gaussian smearing of width 0.1 eV is used [4, 16, 23]. The initial crystal structure of the alloy compound is obtained by replacing one of the metal atoms by other metal atom in the structure of MN_6 (M is transition metal) of Refs.[16, 17].

The mechanical properties are studied by calculating the elastic constants. The elastic constants calculations are performed by using the components of Hessian matrix, which is obtained by applying six finite distortions of lattice followed by stress-strain relationship. The bulk modulus (B) and shear modulus (G) are obtained by using stiffness tensor (C_{ij}) and compliance tensor (S_{ij})

according to Voigt-Reuss-Hill approximations described by the following equations[4, 16, 23, 38-42]. The subscripts V and R denote Voigt and Reuss approximations, respectively.

$$B_V = [(C_{11} + C_{22} + C_{33}) + 2(C_{12} + C_{23} + C_{31})]/9 \quad (1)$$

$$G_V = [(C_{11} + C_{22} + C_{33}) - (C_{12} + C_{23} + C_{31}) + 3(C_{44} + C_{55} + C_{66})]/15 \quad (2)$$

$$B_R = [(S_{11} + S_{22} + S_{33}) + 2(S_{12} + S_{23} + S_{31})]^{-1} \quad (3)$$

$$G_R = 15[4(S_{11} + S_{22} + S_{33}) - 4(S_{12} + S_{23} + S_{31}) + 3(S_{44} + S_{55} + S_{66})]^{-1} \quad (4)$$

$$B = (B_V + B_R)/2 \text{ and } G = (G_V + G_R)/2 \quad (5)$$

Pugh's ratio ($k = G/B$), Poisson's ratio ($\nu = (3 - 2k)/(6 + 2k)$), and Young's modulus ($E = 9G/(3 + k)$) are calculated using B and G. The Vickers hardness (H_V) is determined using the equation that depends on the macroscopic properties (B and G), proposed by Tian et al.,[40-46] as:

$$H_V = 0.92k^{1.137}G^{0.708} \quad (6)$$

Depending on B and G, the Debye temperature (θ_D) is also calculated for the compound with n atoms per unit cell. The transverse ($v_t = \sqrt{G/\rho}$) and longitudinal ($v_l = \sqrt{(3B + 4G)/3\rho}$) components of speed of sound are calculated and following equation is used to estimate θ_D[4, 5, 16, 23, 42]:

$$\theta_D = \frac{h}{k_B}\left[\frac{3n}{4\pi}\left(\frac{\rho N_A}{M}\right)\right]^{1/3}\left[\frac{1}{3}\left(\frac{2}{v_t^3} + \frac{1}{v_l^3}\right)\right]^{-1/3}, \quad (7)$$

where h is Planck's constant, k_B is Boltzmann constant, and N_A is Avogadro number, M is molecular mass, and ρ is density of the material.

The crystal structure is optimized by relaxing the atomic positions, cell volume and shape. The formation energy per formula unit (ΔE_f) of the relaxed cell is calculated using the following equation:

$$\Delta E_f = E(M1_xM2_yN_z) - xE(M1) - yE(M2) - zE(N_2)/2. \quad (8)$$

Here, $M1$ and $M2$ are two different metals, and x, y, and z are positive integers. $E(M1_xM2_yN_z)$, $E(M1)$, $E(M2)$, and $E(N_2)$ are ground state energies of alloy, transition metals, and nitrogen dimer in vacuo[4, 5, 16, 20, 23] obtained from the full relaxation of respective unit cells.

Further, the vibrational stability of crystal structure is determined by calculating the phonon density of states (DOS)[4, 5, 16, 20, 23, 47, 48]. The study of electronic DOS and band gap calculations are also performed by calculating LDOS and band structure curves[4, 6, 16, 17, 21, 23, 49, 50]. The chemical bonding among the atoms is analyzed by: (i) calculating the COHP and (ii) the charge transfer from metal to nitrogen using Bader charge analysis[51-58].

III. RESULTS AND DISCUSSION

A. Structural and vibrational properties

The arrangements of nitrogen and transition metal atoms are presented in the geometrically optimized structure of the crystal in Fig. 1[59]. In this figure, out of total number of metal atoms, the first metal (M1) and second metal (M2) occupy 2/3 and 1/3 atomic sites respectively. Fig. 1 shows the hexagonal ring of nitrogen atoms arranged in the armchair like structure and the distance between two adjacent nitrogen atoms in the ring is predicted to be 1.46 Å for all compounds. This result matches with the earlier theoretically calculated bond length for the N-N pair for other TMNs[14, 16, 17, 60]. This ring formed by strong N-N covalent bonds is the reason for high hardness observed in other TMNs[14, 16, 60]. Table I shows the predicted values of lattice constants *a* (Å) and *c* (Å) for all compounds in hexagonal axes. Table II shows the calculated densities (ρ in kg/m^3) for these materials, which range from 6759 kg/m^3 to 8719 kg/m^3. Table II also shows that in both alloy compounds of W or Mo with Ta, increasing W or Mo increases the hardness, which is expected. This is consistent with the result of compounds of W and Mo where increasing W leads

to increasing hardness (Table II). The results of the variation of volume of the unit cell (V) and formation energies (E_f) for each compound are shown in Fig. 2. The V for each compound (Fig. 2(a)), is found to be increasing with increasing number of W or Mo (for $W_{1-x}Ta_xN_6$ and $Mo_{1-x}Ta_xN_6$) and W (for $W_{1-x}Mo_xN_6$) (x in Fig. 2). In Fig. 2(b), for the nitrides formed with combination of Ta and W ($W_{1-x}Ta_xN_6$, red line with solid circle) or Ta and Mo ($Mo_{1-x}Ta_xN_6$, blue line with solid square), E_f decreases with increasing x. However, those formed by the combination of W and Mo ($W_{1-x}Mo_xN_6$, green line with solid triangle, Fig. 2(b)), E_f increases with increasing x. The each compound. The synthesis of these alloys can be tricky because of the positive E_f values. However, following the synthesis routes implemented by Gregoryanz et. al[13] and Cowhurst et. al,[14] in the synthesis of PtN and PtN_2 where the high pressure of 50 GPa and temperature of 2000 K are used, we believe there is a possibility of synthesizing such materials.

To study the vibrational stability of these compounds, the phonon DOS calculations are performed. The presence of phonon DOS in the imaginary frequency region signifies the material is vibrationally unstable and such materials cannot be quenchable in to the ambient conditions[61]. Our study of phonon frequency calculations is shown in Fig. 3. It is evident from Fig. 3 that only one compound $W_{0.33}Ta_{0.66}N_6$ has significant degree of phonon DOS present in the imaginary frequency region indicating that it is vibrationally unstable compound, all other compounds are vibrationally stable. Fig. 3 also shows that there is little or no gap in the distribution of phonon DOS frequencies. Thus, these materials may not be useful as sound reflector in applications[62].

B. Mechanical properties

The study of mechanical properties is accomplished by calculating B and G. Equations (1) – (5) as described in section II are used to calculate these quantities. The stiffness tensor (C_{ij}) may

be described by five independent elastic constants viz, C_{11}, C_{12}, C_{13}, C_{33}, and C_{44} as the compound has hexagonal symmetry. The predicted values of all these elastic constants are presented in Table I. The components of the compliance tensor (S_{ij}) are calculated by taking the inverse of the C_{ij} tensor. For hexagonal symmetry, material with their C_{ij} values satisfying the conditions $C_{11} > |C_{12}|$, $C_{44} > 0$, and $(C_{11} + 2C_{12})C_{33} > 2C_{13}^2$ are expected to be mechanically stable[4, 6, 16, 23, 38, 40, 63]. Subjected to these conditions, all our compounds are found to be mechanically stable. Elastic moduli and Vickers hardness are computed by using the equations described in section II. The predicted Vickers hardnesses and elastic moduli are presented in Table II. The predicted values for H_V range from 46 GPa ($Mo_{0.33}Ta_{0.66}N_6$) to 55 GPa ($W_{0.66}Ta_{0.33}N_6$ and $W_{0.66}Mo_{0.33}N_6$). These H_V values are above 40 GPa and hence these materials may be regarded as new super hard compounds[25]. Also, for both mechanically and vibrationally stable compounds, the compounds with W as one of the components have H_V greater than 50 GPa. Fig. 2(c) shows the variation of B with x and it is not monotonic. For example, B first decreases and attain its minimum value and then increases with x for $Mo_{1-x}Ta_xN_6$ (blue line with solid square) while for $W_{1-x}Mo_xN_6$, it is generally decreasing (green line with solid triangle). However, it is hard to predict trend of B for $W_{1-x}Ta_xN_6$ (red line with solid circle) with x. The results of our study for variations of G, k, and H_V with x are shown in Fig. 4. The study shows that all G, k, and H_V generally decrease with increasing x and this is expected as the material gets softer, the volume gets bigger (Fig. 2(a)). The predicted values of k are presented in Table II. These values of k are greater than 0.57 for all compounds indicating that these compounds are brittle in nature, as expected[4, 16, 23, 38, 64-66].

We have predicted θ_D only based on the calculated values of B and G by using equation (7) discussed in section II. The predicted θ_D are in the range of 995 K ($W_{0.33}Ta_{0.66}N_6$) to 1151 K ($W_{0.33}Mo_{0.66}N_6$) as presented in Table II. We can also see that the predicted values of θ_D for both

mechanically and vibrationally compounds are always higher than 1000 K indicating the higher melting temperature for these compounds. Studies have shown that θ_D can be predicted from H_V using the relation: $\theta_D = aH_V^{1/2}\rho^{-1/6}M^{-1/3} + b$, where a and b are linear fitting constants, ρ is density of material, and M is molecular weight[4, 16, 23, 67, 68]. We compared our calculated θ_D with this equation and result is shown in Supplementary Fig. S1[69] where we can see the calculated θ_D agrees with the fitted straight line of above equation. The fitting constants a and b are evaluated to be 4908.92 ($\mathrm{GPa}^{-1/2}(\mathrm{kg/m^3})^{1/6}(\mathrm{g/mol})^{1/3}\mathrm{K}$) and 181.80 (K) respectively.

We also predicted the magnetic moments for these compounds in terms of μ_B and the results are shown in Table I. Out of 6 compounds studied, only 4 are magnetic and one of them, $W_{0.33}Ta_{0.66}N_6$, is only mechanically stable but vibrationally unstable. It is interesting to note that all the compounds formed with the combination with W atom are magnetic. For both mechanically and vibrationally stable compounds, the highest magnetic moment per transition metal atom (0.82 μ_B) is observed for $W_{0.66}Mo_{0.33}N_6$ while for remaining two, magnetic moment is negligible.

C. Electronic properties

The study of the charge transfer from metal to nitrogen is performed by utilizing the Bader charge analysis. The calculated values of charge transfer (Q_t) is presented in Table I. It shows a trend of decreasing Q_t when the second metal atom in the compounds increases. For example, Q_t decreases when Ta increases in $W_{1-x}Ta_xN_6$ or $Mo_{1-x}Ta_xN_6$ and Mo increases in $W_{1-x}Mo_xN_6$. We also note from Supplementary Fig. S2 that the calculated Q_t are always higher than their corresponding end members. As H_V for these alloys remains in between their respective end members, it is hard to predict any direct relationship between Q_t and H_V including the end members. However, it is evident from Table II that increasing H_V is attributed to increasing Q_t

for each of these alloys (i.e., excluding end members). This may be the reason that the stronger electrovalent bonding provided by the charge transfer leads to a higher hardness in these compounds.

The LDOS per atom computed for both mechanically and vibrationally stable compounds in the order of increasing hardness from top to bottom are shown in Fig. 5. The results of LDOS above Fermi level show that the widening of population of LDOS for both metal and nitrogen from softest ($Mo_{0.33}Ta_{0.66}N_6$, $H_V = 46$ GPa) to hardest compound ($W_{0.66}Ta_{0.33}N_6$, $H_V = 55$ GPa). The gap in the LDOS above the Fermi level becomes narrower and shifts toward the left as the hardness increases with an exception for the $W_{0.66}Ta_{0.33}N_6$ where it shifts towards right. We also observe the compounds formed by W and Mo have no LDOS at Fermi level showing the non-metallic character whereas the compounds formed with Ta have some LDOS at the Fermi level indicating the metallic nature. As WN_6 and MoN_6 have a band gap and TaN_6 shows metallic character[16, 17], it can be concluded that the alloying of two different TMNs that show semiconducting character in its pure MN_6 form would result in a semiconducting character. We observe in Fig. 5 that below the Fermi level with the increase in hardness: (i) discreteness and peaks of LDOS decrease and (ii) the metallic LDOS for the two metals in any alloy tend to overlap. For metallic compounds it is observed that the population of nitrogen LDOS is higher than the population of metallic LDOS at the Fermi level. This type of trend is typically seen in case of cubic MN_6 materials[4].

We have performed -pCOHP analysis to investigate the bonding and anti-bonding states for metal (M) and nitrogen (N) atoms. The calculated -pCOHP for both mechanically and vibrationally stable compounds are presented in Fig. 6 in the order of increasing hardness from top to bottom. In these figures, the bonding states are represented by the presence of population of -pCOHP above the energy axis (baseline) while those below the baseline denote the anti-bonding

states below the Fermi level. Fig. 6 shows that the M-N interactions are mostly in bonding states (blue, green, or purple lines). Like M-N, N-N interactions are also in bonding states, however, they are in antibonding states near the Fermi level (red line). Our analysis shows the presence of fewer anti-bonding states in M-N interactions for softer compounds, these states decrease with increase in hardness below the Fermi level. These M-N interactions may be providing the extra hardness observed as it can be verified by the existence of charge transfer between M and N atoms discussed earlier. The anti-bonding in N-N interactions is observed to be occurring around -4 eV for all the compounds and it extends up to the Fermi level.

To further understand the electronic properties and its connection with hardness, we have calculated the electronic band structure and band gaps using GGA functional and the results are shown in Fig. 7 for both mechanically and vibrationally stable compounds. This calculation shows that only two materials $W_{0.33}Mo_{0.66}N_6$ and $W_{0.66}Mo_{0.33}N_6$ show the existence of a band gap and the remaining three materials possess metallic character. This result can be verified from LDOS calculations as well (see Fig. 5). Our calculations showed that the predicted band gap for $W_{0.33}Mo_{0.66}N_6$ and $W_{0.66}Mo_{0.33}N_6$ are 1.36 and 1.40 eV respectively, expected to be underestimated as they are calculated by using GGA[21]. To find more accurate band gaps, we calculated these values by using Heyd-Scuseria-Ernzerhof (HSE06) hybrid functional. These predicted values of band gaps show some increment to the previously calculated values ($W_{0.33}Mo_{0.66}N_6$, 1.82 eV and $W_{0.66}Mo_{0.33}N_6$, 1.92 eV) which is expected. Based on these results, it is hard to predict any direct relationship between the observed hardness and band structure for these compounds.

IV. SUMMARY AND CONCLUSIONS

In conclusion, we have studied the ternary TMNs by utilizing DFT based first principles calculations. The alloys under study are $W_{1-x}Ta_xN_6$, $Mo_{1-x}Ta_xN_6$, and $W_{1-x}Mo_xN_6$ where $0 \leq x \leq 1$. The reason for taking W, Mo, and Ta to form alloys with nitrogen is these metals are predicted to have $H_V > 40$ GPa in their pure MN_6 form[16]. Our study of phonon DOS calculation shows that except $W_{0.33}Ta_{0.66}N_6$, all other compounds are vibrationally stable. We also check the mechanical stability and find all the alloy compounds are mechanically stable. The calculated H_V for these materials range from 46 GPa ($Mo_{0.33}Ta_{0.66}N_6$) to 55 GPa ($W_{0.66}Ta_{0.33}N_6$ and $W_{0.66}Mo_{0.33}N_6$), showing the characteristics of possible super hard compounds. The predicted θ_D for both mechanically and vibrationally stable brittle super hard alloys are above 1000 K indicating the materials are suitable for high temperature hard coating applications. The charge transfer study indicating the electrovalent nature of bonding between M and N atoms are also supported by the bonding and anti-bonding study performed via COHP analyses for these materials. We also observe an upward bowing of Q_t with respect to x for these alloys compared with their end members. LDOS and band structure analyses reveal that three of the materials are metallic and two are semiconducting. The calculated values of band gaps for $W_{0.33}Mo_{0.66}N_6$ and $W_{0.66}Mo_{0.33}N_6$ are found to be 1.36 and 1.40 eV for GGA and, 1.82 and 1.92 eV for HSE06 hybrid calculations respectively. Most of these compounds are non-magnetic except $W_{0.66}Mo_{0.33}N_6$, for which magnetic moment per unit transition metal is 0.82 μ_B.

ACKNOWLEDGEMENTS

The computational work for this project is performed at Ohio Super Computer Center . We also thank National Science Foundation Division of Civil, Mechanical, and Manufacturing Innovations through grants 1629239 and 1629230 to support this work.

AUTHOR DECLARATIONS

Conflict of interest

The authors have no conflicts to disclose.

DATA AVAILABILITY

The data that supports the findings of this study are available within the article and its supplementary material.

Table I: Lattice constants (a, c), elastic constants (C_{11}, C_{12}, C_{13}, C_{33}, and C_{44}), charge transfer per atom from metal to nitrogen (Q_t) in units of elementary charge e, and total magnetic moment (Mag.) in Bohr magneton (μ_B) per transition metal atom for all compounds.

Compounds	a (Å)	c (Å)	C_{11} (GPa)	C_{12} (GPa)	C_{13} (GPa)	C_{33} (GPa)	C_{44} (GPa)	Q_t (e)	Mag. (μ_B)
$Mo_{0.66}Ta_{0.33}N_6$	6.19	4.62	652	95	145	723	340	1.32	0
$Mo_{0.33}Ta_{0.66}N_6$	6.21	4.66	649	102	152	703	324	1.29	0
$W_{0.66}Ta_{0.33}N_6$	6.18	4.61	667	71	145	780	365	2.63	-0.13
$W_{0.33}Ta_{0.66}N_6$	6.20	4.65	687	111	164	728	338	2.42	0.23
$W_{0.66}Mo_{0.33}N_6$	6.16	4.57	711	94	147	783	376	1.42	0.82
$W_{0.33}Mo_{0.66}N_6$	6.17	4.58	693	91	144	756	366	1.29	-0.06

Table II: Bulk modulus (B), shear modulus (G), Young's modulus (E), Vickers hardness (H_V), Pugh's ratio (k), Poisson's ratio (ν), Debye temperature (θ_D), formation energy per atom (E_f), and mass density (ρ) for all mechanically stable compounds.

Compounds	B (GPa)	G (GPa)	E (GPa)	H_V (GPa)	k	ν	θ_D (K)	E_f (eV)	ρ (kg/m^3)
$Mo_{0.66}Ta_{0.33}N_6$	310	297	675	49	0.96	0.14	1115	0.97	6759
$Mo_{0.33}Ta_{0.66}N_6$	313	287	660	46	0.92	0.15	1032	0.87	7576
$W_{0.66}Ta_{0.33}N_6$	313	317	712	55	1.01	0.12	1016	0.94	8719
$W_{0.33}Ta_{0.66}N_6$	331	300	692	47	0.91	0.15	995	0.86	8552
$W_{0.66}Mo_{0.33}N_6$	331	329	741	55	0.99	0.13	1092	1.05	7899
$W_{0.33}Mo_{0.66}N_6$	321	320	721	54	1.00	0.13	1151	1.07	6910

Fig. 1: Structure of compound $M1_{2/3}M2_{1/3}N_6$, prepared by using VESTA[59], showing (a) hexagonal ring and (b) armchair like structure of nitrogen (N) atoms. M1 and M2 represent two different metals. **a**, **b**, and **c** represent the crystallographic directions.

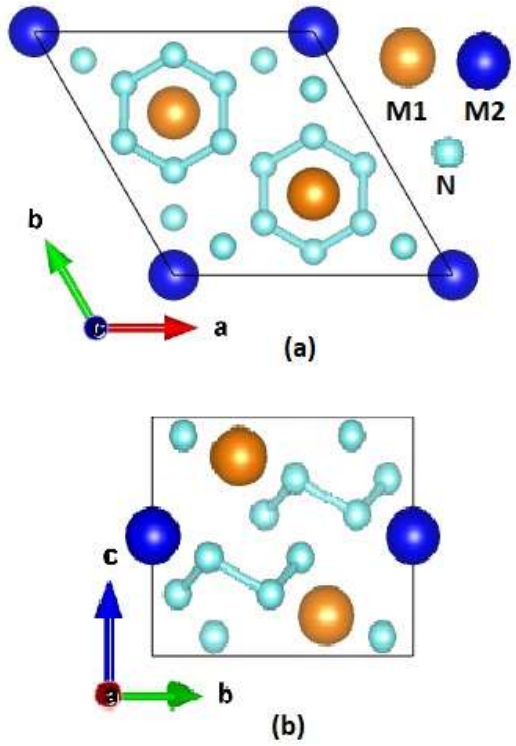

Fig. 2: Study of variation of (a) volume (V), (b) formation energy per atom (E_f) and (c) bulk modulus (B), with increasing number of atoms (x) from second metal.

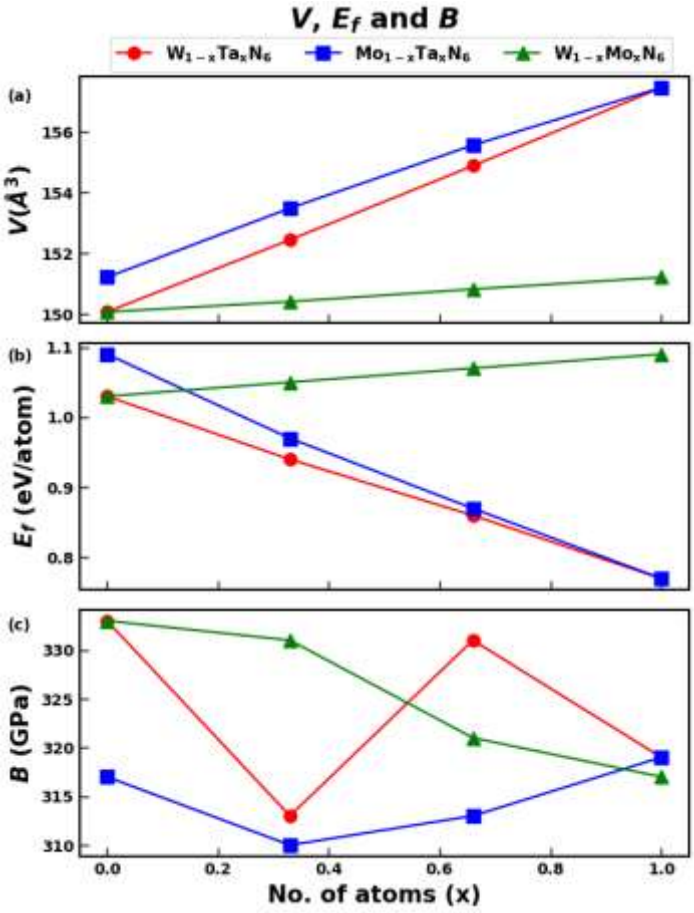

Fig. 3: Comparison of phonon DOS for all mechanically stable compounds, hardness increases from left to right in each panel.

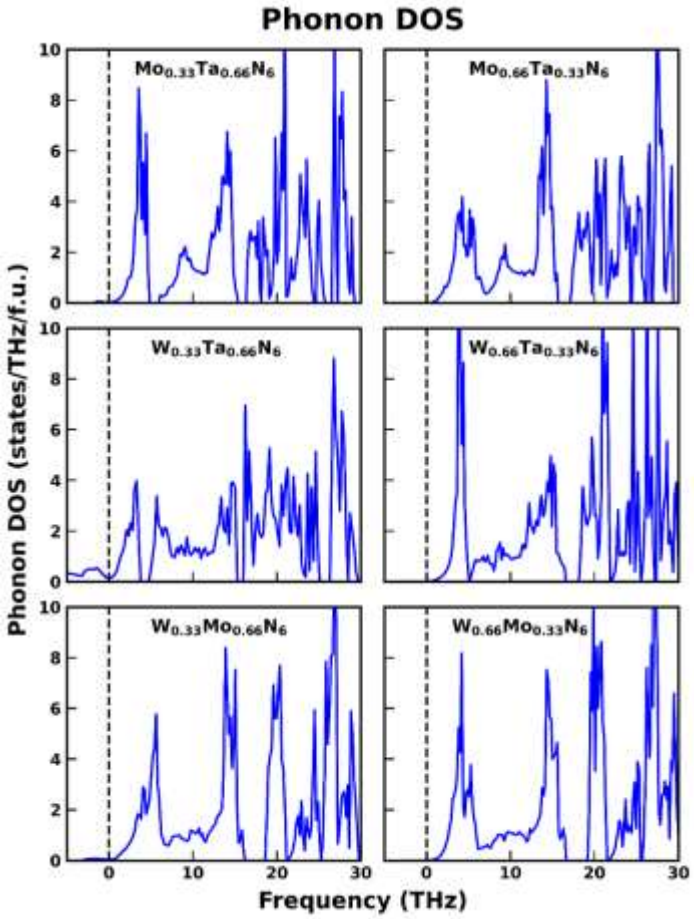

Fig. 4: Study of variation of (a) shear modulus (G), (b) Poisson ratio (k), and (c) Vickers hardness (H_V) with increasing numbers of atoms (x) from second metal.

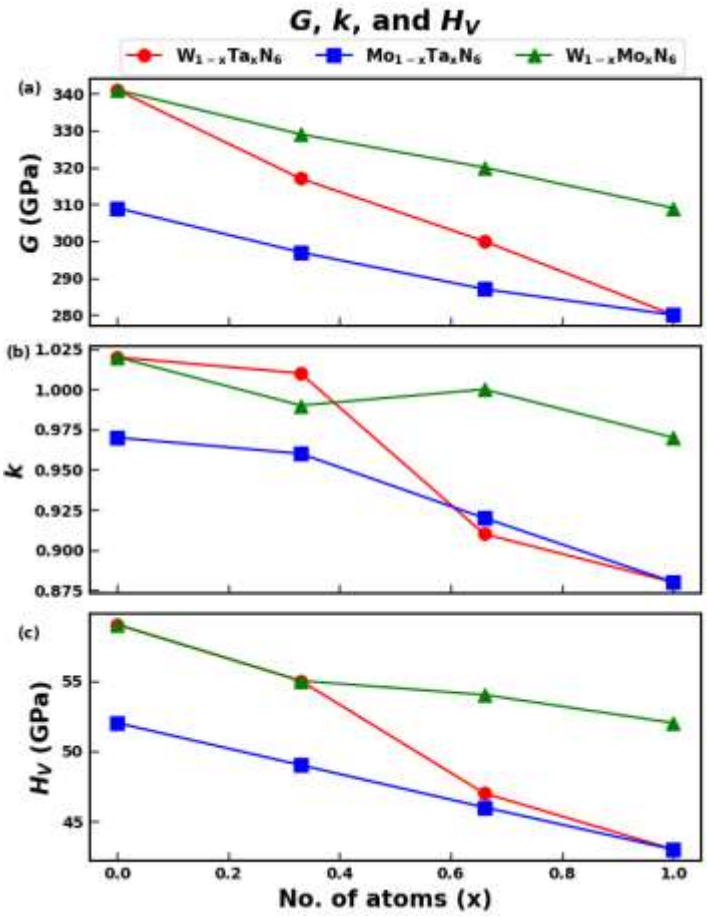

Fig. 5: Comparison of LDOS for both mechanically and vibrationally stable compounds in the order of increasing hardness from top to bottom. The Fermi level is set at 0 eV.

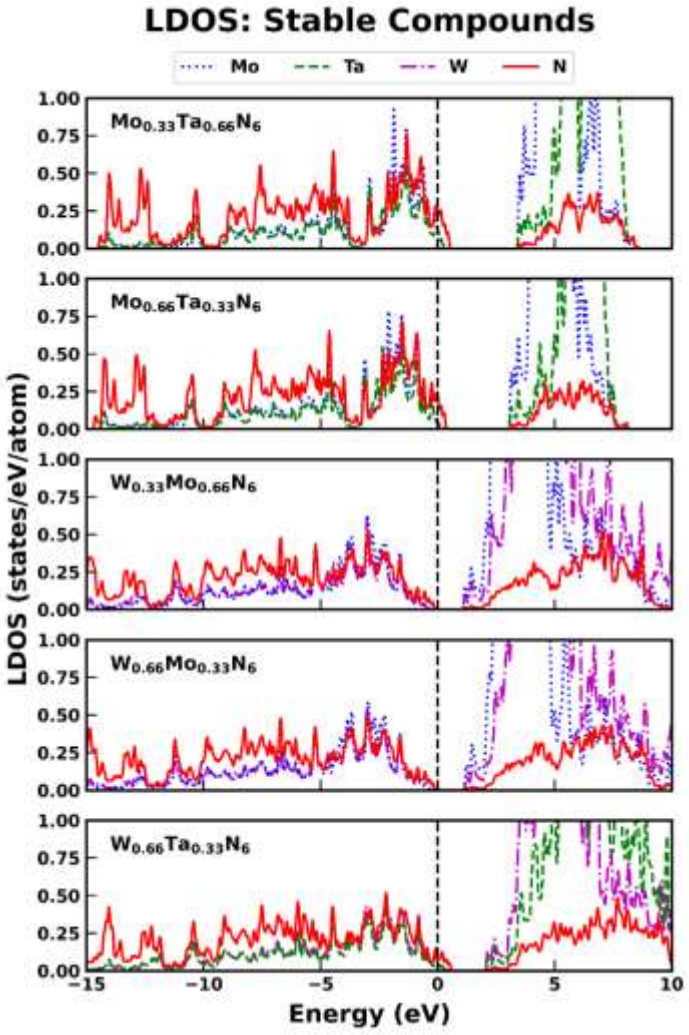

Fig. 6: Comparison of -pCOHP for both mechanically and vibrationally stable compounds in the order of increasing hardness from top to bottom. The Fermi level is set at 0 eV.

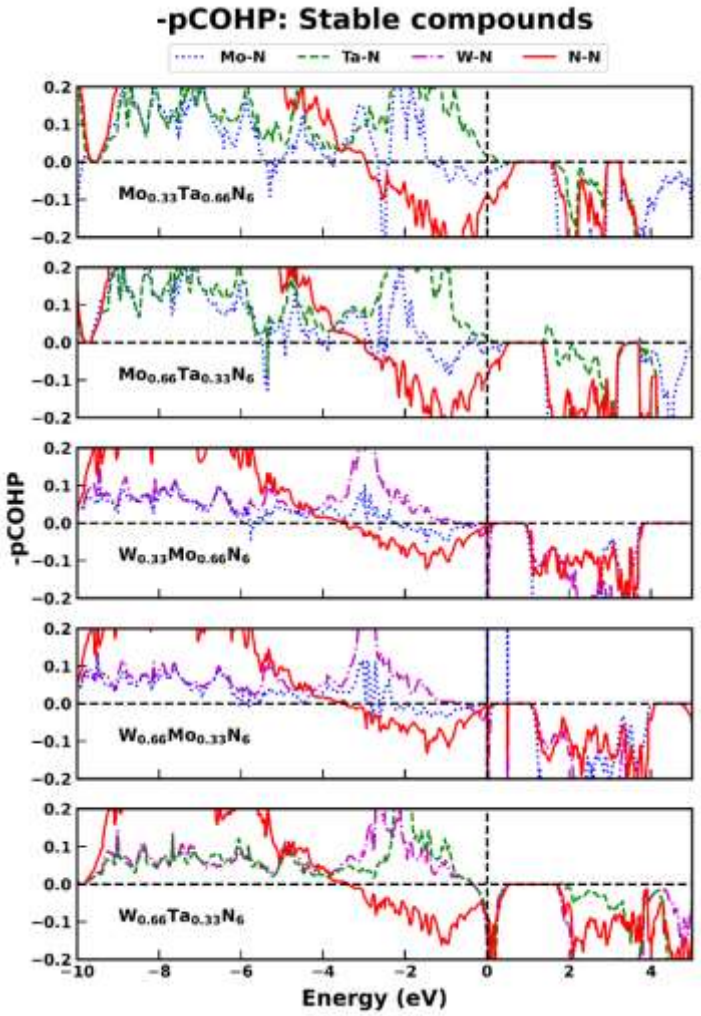

Fig. 7: Electronic band structure curves for both mechanically and vibrationally stable compounds in the order of increasing hardness from top to bottom. The Fermi level is set at 0 eV.

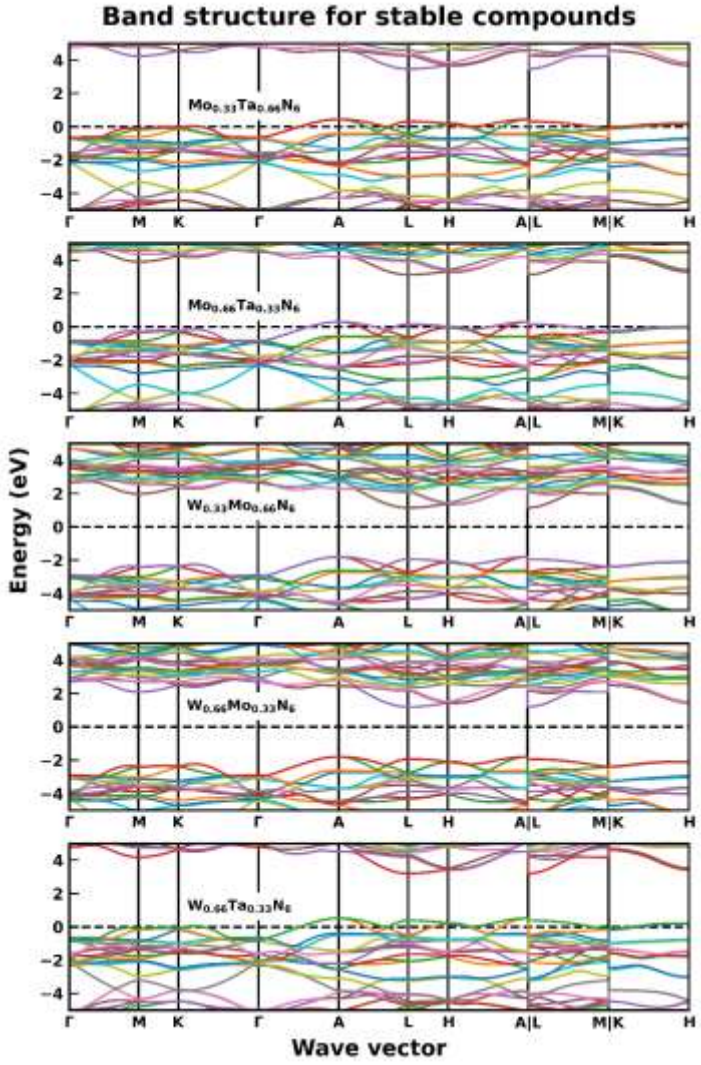

REFERENCES

1. X. J. Chen, V. V. Struzhkin, Z. G. Wu, M. Somayazulu, J. Qian, S. Kung, A. N. Christensen, Y. S. Zhao, R. E. Cohen, H. K. Mao and R. J. Hemley, Proc. Natl. Acad. Sci. U. S. A. **102**, 3198-3201 (2005).

2. S. H. Jhi, S. G. Louie, M. L. Cohen and J. Ihm, Phys. Rev. Lett. **86**, 3348-3351 (2001).

3. Z. T. Y. Liu, X. Zhou, D. Gall and S. V. Khare, Comput. Mater. Sci. **84**, 365-373 (2014).

4. S. R. Kandel, B. B. Dumre, D. Gall and S. V. Khare, J. Phys. Chem. Solids **171**, 111022 (2022).

5. V. Adhikari, Z. T. Y. Liu, N. J. Szymanski, I. Khatri, D. Gall, P. Sarin and S. V. Khare, J. Phys. Chem. Solids **120**, 197-206 (2018).

6. B. B. Dumre, N. J. Szymanski, V. Adhikari, I. Khatri, D. Gall and S. V. Khare, Solar Energy **194**, 742-750 (2019).

7. S. Kodambaka, S. V. Khare, V. Petrova, D. D. Johnson, I. Petrov and J. E. Greene, Phys. Rev. B **67**, 035409 (2003).

8. S. Kodambaka, V. Petrova, S. V. Khare, D. Gall, A. Rockett, I. Petrov and J. E. Greene, Phys. Rev. Lett. **89**, 176102 (2002).

9. S. Kodambaka, V. Petrova, S. V. Khare, D. D. Johnson, I. Petrov and J. E. Greene, Phys. Rev. Lett. **88**, 146101 (2002).

10. H. Chen, F. Peng, H.-k. Mao, G. Shen, H.-P. Liermann, Z. Li and J. Shu, J. Appl. Phys. **107**, 113503 (2010).

11. A. Zerr, N. Chigarev, R. Brenner, D. A. Dzivenko and V. Gusev, physica status solidi (RRL) - Rapid Research Letters **4**, 353-355 (2010).

12. A. Kobayashi, Surf. Coat. Technol. **132**, 152-157 (2000).

13. E. Gregoryanz, C. Sanloup, M. Somayazulu, J. Badro, G. Fiquet, H.-k. Mao and R. J. Hemley, Nat. Mater. **3**, 294-297 (2004).

14. J. C. Crowhurst, A. F. Goncharov, B. Sadigh, C. L. Evans, P. G. Morrall, J. L. Ferreira and A. J. Nelson, Science **311**, 1275-1278 (2006).

15. I. Efthimiopoulos, Z. T. Y. Liu, S. V. Khare, P. Sarin, T. Lochbiler, V. Tsurkan, A. Loidl, D. Popov and Y. Wang, Phys. Rev. B **92**, 064108 (2015).

16. S. R. Kandel, B. B. Dumre, D. Gall and S. V. Khare, Materialia **25**, 101550 (2022).

17. K. Xia, H. Gao, C. Liu, J. Yuan, J. Sun, H.-T. Wang and D. Xing, Science Bulletin **63**, 817-824 (2018).

18. Q. Li, L. Sha, C. Zhu and Y. Yao, EPL (Europhysics Letters) **118**, 46001 (2017).

19. H. Holleck, J. Vac. Sci. Technol. A **4**, 2661 (1986).

20. V. Adhikari, N. J. Szymanski, I. Khatri, D. Gall and S. V. Khare, Thin Solid Films **688**, 137284 (2019).

21. B. B. Dumre and S. V. Khare, Physica B: Condensed Matter **637**, 413896 (2022).

22. N. J. Szymanski, V. Adhikari, M. A. Willard, P. Sarin, D. Gall and S. V. Khare, J. Appl. Phys. **126**, 093903 (2019).

23. S. R. Kandel, B. B. Dumre, D. Gall and S. V. Khare, Comput. Mater. Sci. **221**, 112084 (2023).

24. N. J. Szymanski, Z. T. Y. Liu, T. Alderson, N. J. Podraza, P. Sarin and S. V. Khare, Comput. Mater. Sci. **146**, 310-318 (2018).

25. H. J. McSkimin and W. L. Bond, Physical Review **105**, 116-121 (1957).

26. G. Kresse and D. Joubert, Phys. Rev. B **59**, 1758-1775 (1999).

27. G. Kresse and J. Furthmuller, Comput. Mater. Sci. **6**, 15-50 (1996).

28. G. Kresse and J. Furthmuller, Phys. Rev. B **54**, 11169 (1996).

29. G. Kresse and J. Hafner, Phys. Rev. B: Condens Matter **47**, 558-561 (1993).

30. G. Kresse and J. Hafner, Phys. Rev. B: Condens Matter **49**, 14251-14269 (1994).

31. Y. Wang, Z. T. Y. Liu, S. V. Khare, S. A. Collins, J. Zhang, L. Wang and Y. Zhao, Appl. Phys. Lett. **108**, 061906 (2016).

32. P. P. Gunaicha, S. Gangam, J. L. Roehl and S. V. Khare, Solar Energy **102**, 276-281 (2014).

33. P. E. Blochl, O. Jepsen and O. K. Andersen, Phys. Rev. B: Condens Matter **49**, 16223-16233 (1994).

34. S. V. Khare and T. L. Einstein, Surf. Sci. **314**, L857-L865 (1994).

35. J. P. Perdew, K. Burke and M. Ernzerhof, Phys. Rev. Lett. **77**, 3865-3868 (1996).

36. J. A. Warner, S. K. R. Patil, S. V. Khare and K. C. Masiulaniec, Appl. Phys. Lett. **88**, 101911 (2006).

37. N. Jiang, J. L. Roehl, S. V. Khare, D. G. Georgiev and A. H. Jayatissa, Thin Solid Films **564**, 331-338 (2014).

38. Q. Wei, C. Zhao, M. Zhang, H. Yan and B. Wei, Phys. Lett. A **383**, 2429-2435 (2019).

39. R. Hill, Proc. Phys. Soc. **65**, 349-354 (1952).

40. Z.-j. Wu, E.-j. Zhao, H.-p. Xiang, X.-f. Hao, X.-j. Liu and J. Meng, Phys. Rev. B **76**, 054115 (2007).

41. V. T. Barone, B. B. Dumre, B. R. Tuttle and S. V. Khare, J. Appl. Phys. **131**, 205701 (2022).

42. Z. T. Liu, X. Zhou, S. V. Khare and D. Gall, J. Phys.: Condens Matter **26**, 025404 (2014).

43. R. S. Touzani and M. Krüger, Crystals **10**, 865 (2020).

44. X. Zhou, D. Gall and S. V. Khare, J. Alloys Compd. **595**, 80-86 (2014).

45. Y. Tian, B. Xu and Z. Zhao, Int. J. Refract. Met. Hard Mater. **33**, 93-106 (2012).

46. W. Bao, D. Liu and Y. Duan, Ceram. Int. **44**, 14053-14062 (2018).

47. Z. T. Y. Liu, D. Gall and S. V. Khare, Phys. Rev. B **90**, 134102 (2014).

48. A. Togo and I. Tanaka, Scripta Materialia **108**, 1-5 (2015).

49. R. Deng, B. D. Ozsdolay, P. Y. Zheng, S. V. Khare and D. Gall, Phys. Rev. B **91**, 045104 (2015).

50. B. B. Dumre, D. Gall and S. V. Khare, J. Phys. Chem. Solids **153**, 110011 (2021).

51. M. Yu and D. R. Trinkle, J. Chem. Phys. **134**, 064111 (2011).

52. E. Sanville, S. D. Kenny, R. Smith and G. Henkelman, J. Comput. Chem. **28**, 899-908 (2007).

53. W. Tang, E. Sanville and G. Henkelman, J. Phys.: Condens Matter **21**, 084204 (2009).

54. G. Henkelman, A. Arnaldsson and H. Jónsson, Comput. Mater. Sci. **36**, 354-360 (2006).

55. V. L. Deringer, A. L. Tchougreeff and R. Dronskowski, J. Phys. Chem. A **115**, 5461-5466 (2011).

56. R. Dronskowski and P. E. Bloch, J. Phys. Chem. **97**, 8617-8624 (1993).

57. S. Maintz, V. L. Deringer, A. L. Tchougreeff and R. Dronskowski, J. Comput. Chem. **37**, 1030-1035 (2016).

58. S. Maintz, M. Esser and R. Dronskowski, Acta Physica Polonica B **47**, 1165-1175 (2016).

59. K. Momma and F. Izumi, J. Appl. Crystallogr. **44**, 1272-1276 (2011).

60. R. Yu, Q. Zhan and X. F. Zhang, Appl. Phys. Lett. **88**, 051913 (2006).

61. Z. Zhao, K. Bao, F. Tian, D. Duan, B. Liu and T. Cui, Phys. Rev. B **93**, 214104 (2016).

62. R. M. Hornreich, M. Kugler, S. Shtrikman and C. Sommers, Journal de Physique I **7**, 509-519 (1997).

63. C. M. Kube and M. de Jong, J. Appl. Phys. **120**, 165105 (2016).

64. X. Jiang, J. Zhao and X. Jiang, Comput. Mater. Sci. **50**, 2287-2290 (2011).

65. A. M. Tehrani and J. Brgoch, J. Solid State Chem. **271**, 47-58 (2019).

66. S. F. Pugh, Philos. Mag. J. Sci. **45**, 823-843 (1954).

67. P. Deus and H. A. Schneider, Cryst. Res. Technol. **18**, 491-500 (1983).

68. N. Miao, B. Sa, J. Zhou and Z. Sun, Comput. Mater. Sci. **50**, 1559-1566 (2011).

69. *See Supplementary material [URL will be inserted by AIP Publishing] for Debye temperature (Fig. S1) and charge transfer (Fig. S2) studies.*